A new diagnostic for tropospheric ozone production

Peter M. Edwards[1]* & Mathew J. Evans[1,2]

[1] Wolfson Atmospheric Chemistry Laboratories, Department of Chemistry, University of York, Heslington, York, YO10 5DD, UK

[2] National Centre for Atmospheric Science, Department of Chemistry, University of York, Heslington, York, YO10 5DD, UK

*pete.edwards@york.ac.uk

Abstract

Tropospheric ozone is important for the Earth's climate and air quality. It is produced during the oxidation of organics in the presence of nitrogen oxides. Due to the range of organic species emitted and the chain like nature of their oxidation, this chemistry is complex and understanding the role of different processes (emission, deposition, chemistry) is difficult. We demonstrate a new methodology for diagnosing ozone production based on the processing of bonds contained within emitted molecules, the fate of which is determined by the conservation of spin of the bonding electrons. Using this methodology to diagnose ozone production in the GEOS-Chem chemical transport model, we demonstrate its advantages over the standard diagnostic. We show that the number of bonds emitted, their chemistry and lifetime, and feedbacks on OH are all important in determining the ozone production within the model and its sensitivity to changes. This insight may allow future model-model comparisons to better identify the root causes of model differences.

1. Introduction

The chemistry of the troposphere is one of oxidation [*Levy*, 1973; *Kroll et al.*, 2011]. Organic compounds together with nitrogen and sulfur containing molecules are emitted into the troposphere where they are oxidised into compounds which can either be: absorbed by the biosphere; are involatile enough to form aerosols; can deposit to the surface; or be taken up by clouds and rained out. The oxidation of these compounds is significantly slower than might be expected based on the atmospheric composition of 20% molecular oxygen (O_2).

The inefficiency of ground state O_2 as an atmospheric oxidant is due to its electronic structure. In quantum mechanics, all atomic particles have an intrinsic angular momentum known as spin [*Atkins and De Paula*, 2014]. The spin of an electron is described by the spin quantum number, s, and can have values of either +½ or -½ for a single electron. The Pauli exclusion principle states that if two electrons occupy the same orbital then their spins must be paired, and thus cancel. With two unpaired electrons ground state O_2 is a spin-triplet with a total spin quantum number S=½+½=1 (giving a term symbol of $^3\Sigma_g^-$). In contrast, virtually all trace chemicals emitted into the atmosphere contain only paired electrons and are thus spin-singlets (S=0). The quantum mechanical spin selection rule ΔS=0 means that allowed electronic transitions must not result in a change in electron spin. From a simplistic perspective (i.e. ignoring nuclear spin interactions, inter-system crossings, nuclear dipole effects etc.) this spin selection rule means that the reaction of ground state O_2 with most emitted compounds is effectively spin forbidden. Electronically excited O_2 ($^1\Delta_g$ or $^1\Sigma_g^+$) is a spin singlet and is more reactive in the atmosphere but low concentrations limit its role [*Larson and Marley*, 1999]. Instead, atmospheric oxidation proceeds predominantly via reactions with spin-doublet oxygen-derived species (S=½), notably the hydroxyl (OH) and peroxy radicals (RO_2 = HO_2, CH_3O_2, $C_2H_5O_2$, etc.), or spin-singlet species (e.g. ozone (O_3)).

One of the few spin-triplet species in the atmosphere other than O_2 is the ground state of atomic oxygen ($O(^3P)$), which readily undergoes a spin allowed reaction with O_2 to produce the spin-singlet O_3 molecule. This spin allowed reaction is responsible for the creation of O_3 in both the stratosphere, where it forms the protective O_3 layer, and the troposphere. The ability of O_3 to oxidise other spin-singlet species makes it a powerful oxidant, and it is thus considered a pollutant with negative health effects. Sources of $O(^3P)$ within the troposphere are limited because solar photons at sufficiently short wavelengths to directly photolyse O_2 to $O(^3P)$ are essentially unavailable.

Aside from the photolysis of O_3 itself, the only other significant source of tropospheric $O(^3P)$ is the photolysis of nitrogen dioxide (NO_2) [*Crutzen*, 1971]. Nitrogen oxides are emitted into the troposphere as nitrogen oxide (NO), which can be oxidised to NO_2 by O_3 and other oxidants. A large thermodynamic energy barrier prevents oxidation of NO to NO_2 by the OH radical [*Nguyen et al.*, 1998], and therefore NO oxidation occurs through reaction with either O_3 or RO_2. In terms of O_3

production, the oxidation of NO by O_3 forms a null cycle. Thus only the reaction of NO with RO_2 leads to a net production of O_3.

Exploring the distribution, source and sinks of tropospheric O_3 is a central theme of atmospheric science. Chemical transport models (online and offline) are essential tools enabling this understanding but their validity needs to be continually assessed. Model-model comparison exercises are commonly performed to assess performance, and comparisons of modelled O_3 budgets traditionally form part of this assessment [*Stevenson et al.*, 2006; *Wu et al.*, 2007; *Wild*, 2007; *Young et al.*, 2013]. Ozone production is diagnosed from the flux of NO to NO_2 via reaction with each of the speciated RO_2 in the model's chemical schemes. This approach provides information on the relative importance of the different RO_2 in the fast NO + RO_2 reactions within the model, but gives very little detail on how the longer time scale model processes (emissions, chemistry, deposition) influence O_3 production. Thus exploring the reasons that models differ in their O_3 production is difficult and progress has been slow.

A new diagnostic framework that links large scale model drivers such as emission, chemistry, and deposition to O_3 production would allow an improved assessment of why model ozone budgets differ. We attempt to provide such a framework here.

2. A new diagnostic framework.

The rate of production of tropospheric O_3 is limited by the rate of oxidation of NO to NO_2, which is in turn limited by the rate of production of peroxy radicals (RO_2). Peroxy radicals form through association reactions of hydrogen (H) atoms or alkyl radicals (both spin-doublets, S=½) with O_2, forming a highly reactive spin-doublet radical on an oxygen atom. This spin allowed reaction converts spin-triplet O_2 that cannot react with spin-singlet pollutants into a spin-doublet O_2 containing species that can. As such the formation of RO_2 is central to the atmosphere's oxidation capacity, and its production is limited by the rate of production of H atoms or alkyl radicals. Thus the maximum potential rate of tropospheric O_3 production is equal to the rate at which H atoms and alkyl radicals are produced.

Hydrogen atoms and alkyl radicals are predominantly produced via the spin allowed breaking of the spin-pairing between the two electrons in a C or H containing covalent bond (S=0), such as those in hydrocarbons. These spin-pairings can be broken in the

atmosphere either chemically or photolytically, with the products necessarily conserving spin. The breaking of a covalent bond by a photon (s=1) can result in two products with S=½ or two products with S=0. Likewise, oxidation by a radical (S = ½) will result in one product with S=0 and one with S=½, because the unpaired electron on the radical reactant pairs with one of the covalent bond electrons to produce a spin-singlet.

Although the majority of RO_2 is formed from emitted C or H containing covalent bonds, there are a few notable exceptions. Hydrogen atoms can also be produced through the oxidation of CO to CO_2 by OH. During this reaction the coordinate bond between the C and O atom is broken and the H atom is produced via the breaking of the O-H bond. The other notable exception is the oxidation of an SO_2 lone pair of electrons to SO_3 by OH, where again the H atom produced comes from the OH. In both of these exceptions a spin-singlet electron pairing (CO coordinate bond or SO_2 lone pair) is broken during the production of the H atom, and we can therefore consider these reactions as similar to the breaking of C or H containing covalent bond. For simplicity these spin-singlet electron pairings that can be broken in the troposphere to produce either a H atom or alkyl radical will be referred to as "oxidisable bonds" (C-C, C-H, C=C, CO coordinate bond, S:).

Tropospheric O_3 production occurs through the oxidation of NO by RO_2. Following the above rationale, these RO_2 are produced during the spin allowed breaking of oxidisable bonds predominantly contained within emitted VOCs. This perspective allows us to build a new metric for the production of tropospheric O_3 based around the spin conserving properties of oxidisable bond breaking. In the extreme case, all oxidisable bonds are photolysed to produce two spin-doublet RO_2 products, which then react exclusively with NO to generate O_3. Thus at steady state, the maximum rate of O_3 production is equal to the rate of production of RO_2, which is equal to twice the rate of destruction of the number of oxidisable bonds. This in turn is equal to twice the rate of emission of oxidisable bonds. Deviation from this maximum is determined by:

- The relative importance of processes that produce spin-singlet vs. spin-doublet products during oxidisable bond breaking;
- The fraction of spin-doublet products from oxidisable bond breaking which form RO_2;
- The fraction of RO_2 that go on to oxidize NO to NO_2.

To illustrate this Fig. 1 shows the tropospheric oxidation of a methane (CH_4) molecule through various steps to either a carbon dioxide (CO_2) molecule or a species that is deposited (CH_3OOH, CH_2O, CH_3NO_3). Methane contains 4 x C-H oxidisable bonds (8 paired bonding-electrons) and as the oxidation proceeds, the number of oxidisable bonds decays to zero. Figure 1 highlights the steps in the tropospheric CH_4 oxidation mechanism that form spin-doublet products, with between 1 and 5 RO_2 produced depending on the oxidation pathway. This compares with the theoretical maximum of 8 if all the original C-H bonds were photolysed to yield 2 spin-doublet products.

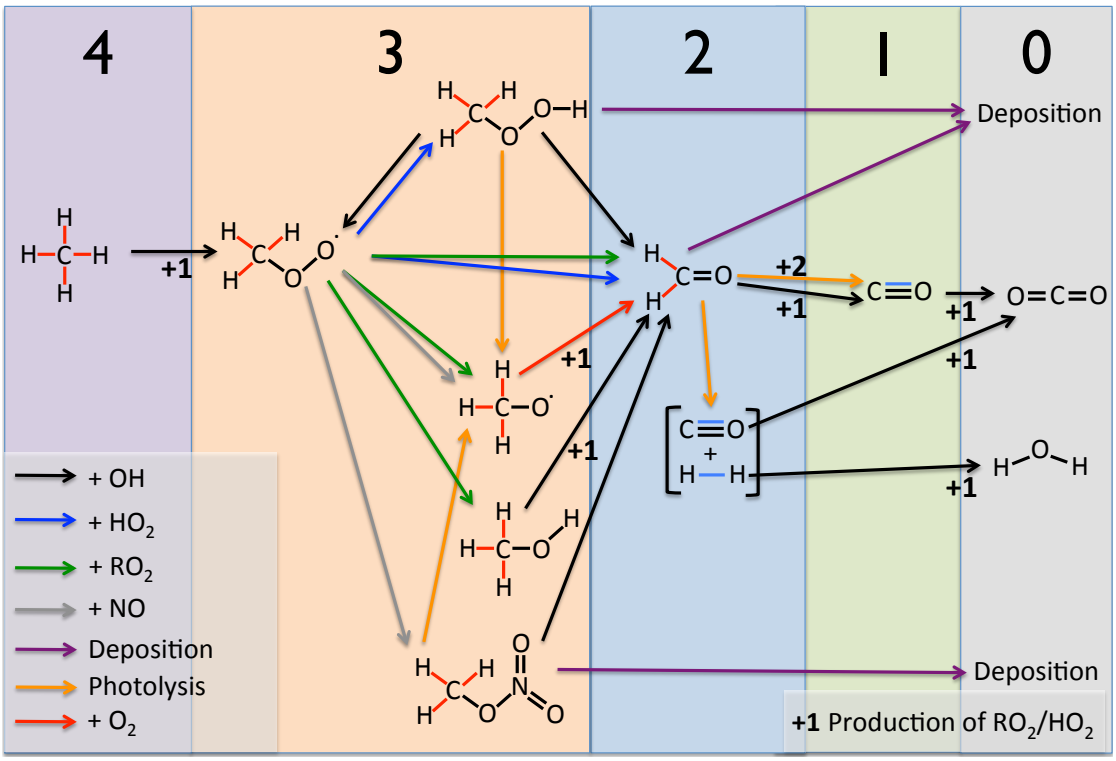

Figure 1. Peroxy radical production during the tropospheric oxidation of CH_4. Moving from left to right, the oxidisable bonds (emitted = red, produced = blue) present in CH_4 are removed via a range of tropospheric processes, indicated by the coloured arrows. The large numbers across the top of the figure indicate the number of oxidisable bonds at each stage of this oxidation. The production of RO_2 is indicated by the +1/+2 numbers with the associated process arrows for producing 1 or 2 RO_2 respectively.

The principal atmospheric source of oxidisable bonds is the emission of C-H, C-C and C=C bonds in hydrocarbons, with the only other significant sources being the emission of CO and the chemical production of CO and H_2 during hydrocarbon oxidation. Over a long enough timescale, the global atmosphere can be considered to

be in a chemical steady state, where the rate of loss of oxidisable bonds is balanced by the rate of production or emission. Thus the O_3 production rate can be described by equation (1), where the O_3 production metric P_sO_3 is equal to the number of spin-paired electrons in oxidisable bonds (i.e. twice the sum of the number of oxidisable bonds emitted (E_{bonds}) and chemically produced (P_{bonds})), multiplied by the number of spin-doublet radicals produced per oxidisable bond break divided by the maximum of 2 ($F_{Radicals}$), multiplied by the fraction of the radicals produced which are RO_2 (F_{RO2}), multiplied by the fraction of RO_2 that goes on to react with an NO to produce an O_3 molecule (F_{NO}). A small correction (I) for the production of RO_2 via reactions of spin-doublet radicals other than those that result in the breaking of oxidisable spin-pairings (e.g. $O_3 + OH \rightarrow HO_2 + O_2$) is included.

$$P_sO_3 = \left(\left(2\times(E_{bonds} + P_{bonds})\times F_{radicals}\times F_{RO_2}\right) + I\right)\times F_{NO} \quad (1)$$

3. Implementation

We use the GEOS-Chem model to evaluate this new O_3 production diagnostic. GEOS-Chem is a global chemical transport model of tropospheric chemistry, aerosol and transport (www.geos-chem.org version 9-02). The model is forced by assimilated meteorological and surface fields (GEOS-5) from NASA's Global Modelling and Assimilation Office, and was run at 4°x5° spatial resolution. The model chemistry scheme includes O_X, HO_X, NO_X, BrO_X and VOC chemistry as described in Mao et al. [2013] as are the emissions. The new P_sO_3 diagnostic has been implemented via the tracking of reactions by type in the GEOS-Chem chemical mechanism file (further details given in the SI). This tracking of reactions enables the fate of all oxidisable bonds as well as the production and loss of all RO_2 within the model to be determined using the standard GEOS-Chem production and loss diagnostic tools. Model simulations were run for 2 years (July 1st 2005 – July 1st 2007) with the first year used as a spin up and the diagnostics performed on the second year.

The standard GEOS-Chem diagnostic for O_3 production (PO_3) is shown on the left side of Table 1. This emphasizes the very fast cycling between NO and NO_2, but provides little in terms of higher process level information. The right side of Table 1 shows the new budget for P_sO_3, which tracks the processing of oxidisable bonds within the model. Both diagnostic methods give the same final answer but our new methodology provides more process level detail. Figure 2 illustrates this new process

based approach, showing the flow of emitted oxidisable spin-paired electrons (bonds) to O_3 and the magnitude of the various mechanisms that contribute to and compete with O_3 production. The annual oxidisable bond emission of 389 T mol yr^{-1} has the potential to create 778 T mol yr^{-1} of radicals. If all oxidisable bonds were broken by photons to produce two radical products the RO_2 production would be 778 T mol yr^{-1}. If the oxidisable bonds were instead broken via radical reaction (e.g. OH) then RO_2 production would be 389 T mol yr^{-1}. The various oxidisable bond breaking / removal pathways within the model result in the production of 280 T mol yr^{-1} of RO_2, with the remainder largely producing stable spin singlet products.

Of the 280 T mol yr^{-1} RO_2 produced, 112 T mol yr^{-1} reacts with NO to produce O_3. The remainder is lost through the reaction or deposition of RO_2 reservoir species (RO_{2y}= RO_2 + peroxides + peroxy-acetyl nitrates). For example the production of methylperoxide (CH_3O_2 + HO_2 = CH_3OOH) results in the loss of 2 RO_2's. However, the reaction of methylperoxide with OH can re-release CH_3O_2 (CH_3OOH + OH = CH_3O_2 + H_2O). Thus, the production of methylperoxide represents the loss of a HO_2 and the movement of a CH_3O_2 into a peroxide RO_{2y} reservoir species. The deposition of a peroxide molecule is thus the loss of a RO_{2y} reservoir species. Notable in Fig. 2 is that the role of PAN and nitrate removal of global RO_{2y} is negligible, instead being dominated by peroxide production and loss and the reaction of RO_2 with O_3.

***P*O$_3$ / T mol Yr^{-1}**		***P*O$_3$ / T mol Yr^{-1}** (except $F_{Radicals}$, F_{RO2}, and F_{NO} which are all unitless)	
NO + HO_2 → NO_2	74	E_{bonds}	330
NO + CH_3O_2 → NO_2	27	P_{bonds}	58
Other RO_2 + NO → NO_2	10	$F_{radicals}$	0.40
Other	1	F_{RO2}	0.86
		Inorganic RO_2 source	15
		F_{NO}	0.40
***P*O$_3$**	**112**	***P*$_s$O$_3$**	**112**

Table 1. Comparison of ozone production diagnostics for GEOS-Chem base simulation. Standard model PO_3 diagnostics (left column) show reactions responsible for NO to NO_2 conversions but provide little process level

information. The new P_sO_3 (right) provides increased information on the processes controlling O_3 production within the model.

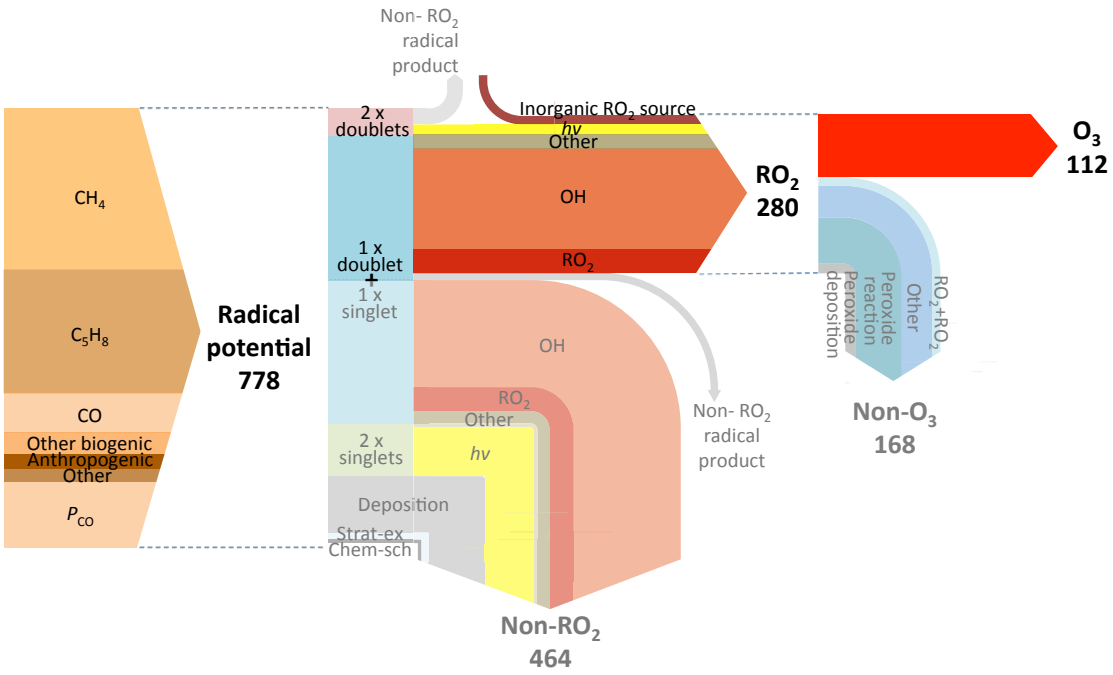

Figure 2. Flow of oxidisable bonds to O_3 production in the GEOS-Chem base simulation. Arrows are coloured according to process and the arrow thickness is proportional to the flux through that channel. Spin-paired electrons are input as oxidisable bonds into the model (left arrow), with the potential to create 778 T mol yr^{-1} of radicals. The actual fate of these bonds is shown in the central arrow, producing 280 T mol yr^{-1} of RO_2, of which 112 T mol yr^{-1} reacts with NO to produce O_3 (right arrow).

3.1 Emitted oxidisable bonds

The fuel for tropospheric oxidation chemistry is the emission of oxidisable bonds, predominantly in the form of hydrocarbons. The production of tropospheric O_3 from the spin-paired bonding electrons emitted into the standard GEOS-Chem model occurs with an efficiency of 14% (112 T mol yr^{-1} molecules of O_3 produced / 778 T mol yr^{-1} spin-paired electrons emitted as oxidisable bonds, Fig.2). These spin-paired bonding electrons are predominantly emitted in the form of CH_4, isoprene (C_5H_8) and CO (37%, 28%, and 9% respectively). Oxidisable bonds produced during chemical reactions (P_{bonds}), account for 15% of the net source. Figure 3 shows emissions of CO and hydrocarbons in the standard GEOS-Chem simulation in terms of mass of carbon per compound, number of oxidisable bonds per compound and as number of bonds in

different oxidisable bond types. The commonly used carbon mass approach splits emissions approximately equally between each of the major sources (CH_4 (29%), Isoprene (32%) and CO (30%)). In contrast, the oxidisable bonds accounting approach apportions hydrocarbon emissions 44%, 33% and 11% for CH_4, isoprene and CO respectively. This highlights the high number of oxidisable bonds per carbon atom in CH_4 (4) compared to isoprene (2.8) and CO (1). Thus efforts to consider emissions on a per-bond basis may provide more insight into chemical processes, as it is these bonds that ultimately determine the chain-like chemistry rather than the mass of carbon atoms. This helps to emphasise the relative importance of CH_4 emissions on global tropospheric chemistry compared with other emissions such as isoprene or CO. The type of oxidisable bond emitted is overwhelmingly C-H (71%).

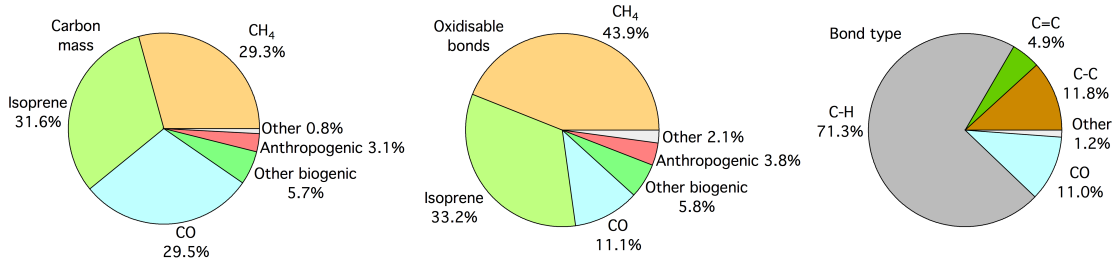

Figure 3. Pie charts showing hydrocarbon emissions in the base GEOS-Chem simulation. Emissions split by carbon mass (left), number of oxidisable bonds (centre) and bond type (right).

The total emission and production of oxidisable bonds has the potential to create 778 T mol yr^{-1} of radicals. However, only 6% of the oxidisable spin-pairings are broken to give the maximum 2 spin-doublet products (e.g. radical channel of CH_2O photolysis). The majority (68%) are oxidized via reaction with a spin-doublet species (OH) to produce 1 spin-singlet and 1 spin-doublet product (e.g. OH + VOC). The remaining 26% of spin-paired electrons are removed to form two spin-singlets (e.g. the non-radical channel of CH_2O photolysis). Thus, of the 778 Tmol yr^{-1} spin-paired electrons emitted or produced only 265 T mol yr^{-1} (34%) are converted into RO_2, with an additional 15 T mol yr^{-1} produced from reactions such as $O_3 + OH \rightarrow HO_2 + O_2$ (*I*). The efficiency of O_3 production from the available oxidisable bonds is further reduced as only 40% of the 280 T mol yr^{-1} of RO_2 produced react with NO to produce NO_2. The remainder is lost either through the self-reaction of RO_2 or via loss through deposition or reaction of RO_{2y} reservoir species (e.g. peroxides). Thus overall 14% of the emitted bonding electrons go on to make O_3.

The new O_3 production diagnostic presented here (P_sO_3) shows the impact of processes such as emission, deposition and chemical mechanism, and provides significantly more detail than the standard PO_3 diagnostic approach (Table 1). We now explore the sensitivity of model O_3 production to changing emissions of NO_x and VOC from the perspective of the two diagnostic methods.

4 Model sensitivities

Understanding model response to changing emissions is an important tool for considering policy interventions. The major controls on O_3 production are emissions of NO_x and VOCs. We show in Fig. 2 that from the perspective of global O_3 production, oxidisable bond emissions are dominated by CH_4 and isoprene. Figure 4 shows the impact of changing emissions of NO_x, isoprene and CH_4 on O_3 production from both the perspective of this new methodology and the conventional $NO+RO_2$ diagnostic approach. A set of 5 simulations was performed for each model sensitivity investigated (NO_x, isoprene and CH_4), with a common base simulation, resulting in 13 simulations in total. The following sections investigate these model responses and use the new diagnostic to provide insight into the processes driving the observed response in O_3 production.

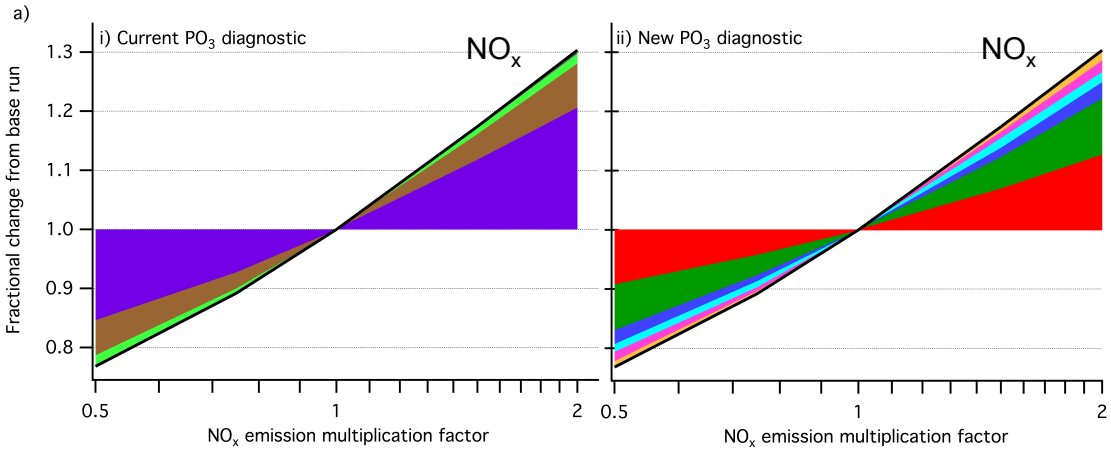

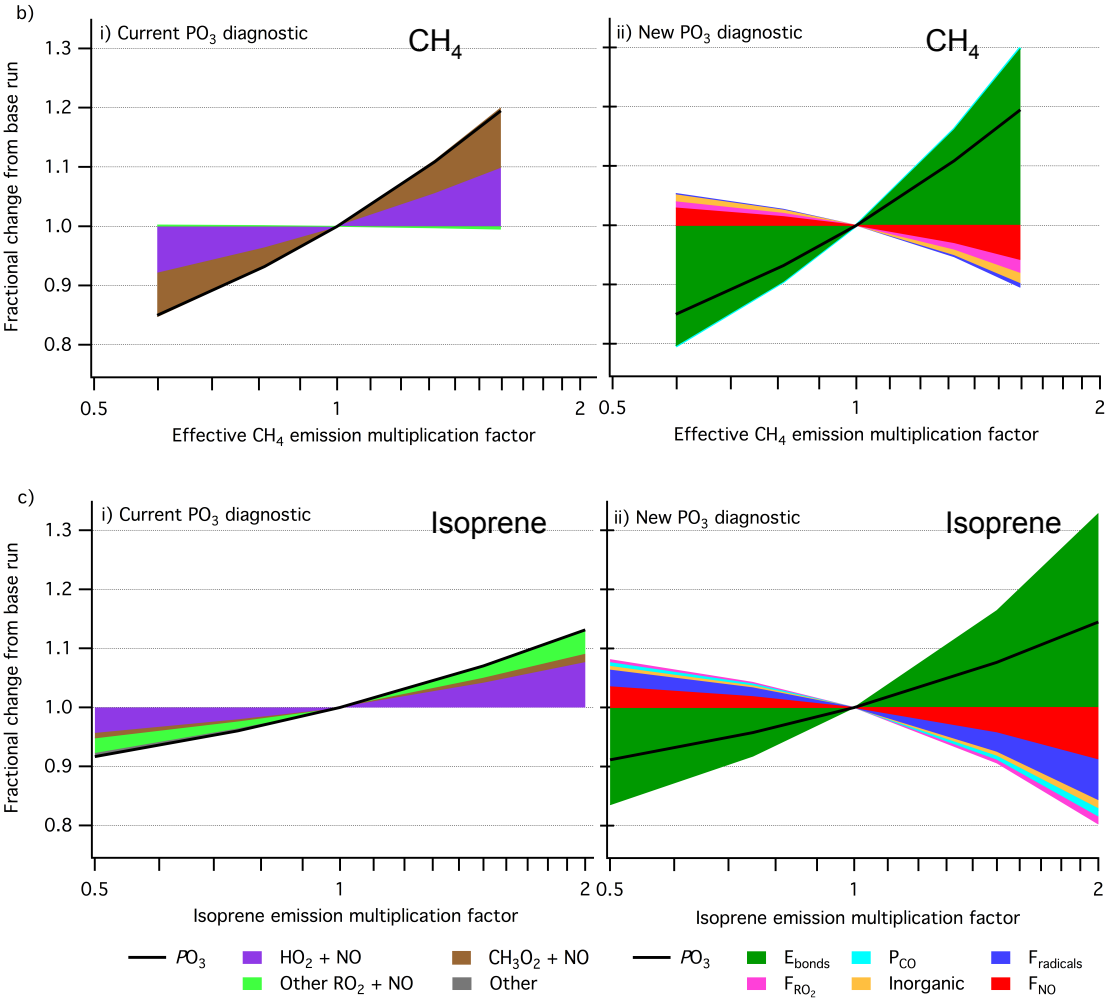

Figure 4. Understanding the effect of NO_x and VOC emissions on ozone production at the process level. Stack plots showing fractional change in model PO_3 compared to base simulation and associated contributions from the current PO_3 (i) and new P_sO_3 (ii) diagnostic parameters under changing NO_x emissions (a), effective CH_4 emission (b) and isoprene emission (c). The P_sO_3 diagnostic parameters are derived for each model simulation using the diagnostic implementation described in Sect. 3, and the fractional change in each parameter from the base simulation calculated.

4.1 NO_x emissions

Figure 4a diagnoses the relative response of GEOS-Chem O_3 production to changing NO_x emissions, using simulations where NO_x emissions from anthropogenic, biomass burning, biofuels, soil and lighting sources were multiplied by factors of 0.5 - 2. Increasing NO_x emissions increases O_3 production. The standard RO_2+NO diagnostic (Fig.4a(i)) shows that fractional contributions to the total change in PO_3 from HO_2

(67%), methyl-peroxy (CH_3O_2) (25%), and other RO_2 (8%) remain approximately constant across the NO_x emission range investigated. This diagnostic provides little detail on the processes driving the change in O_3 production under changing NO_x emissions. In contrast, Fig. 4a(ii) is based on the new P_sO_3 diagnostic and shows a range of process level changes occurring as NO_x emissions change.

4.1.1 Impact of changing NO_x emission on F_{NO}

Unsurprisingly, as NO_x emissions increase the fraction of RO_2 reacting with NO to produce NO_2 (F_{NO}) increases (red section in Fig. 4a(ii)). However, this impact only accounts for around 40% of the increase in P_sO_3. Figure 5a shows the fractional change in all the P_sO_3 efficiency parameters and the global mean NO_x concentration as a function of the changing NO_x emission. As NO_x emissions increase the increase in NO_x concentration in the model is somewhat dampened. Halving the NO_x emission leads to NO_x burdens dropping by ~35%, and doubling leads to an increase of 95%. This dampening is due to the impact of NO_x emissions on OH (see section 4.1.2), which is the dominant sink for NO_x. Increasing NO_x increases OH concentrations, which in turn shortens the NO_x lifetime thus dampening the response of concentration to emission.

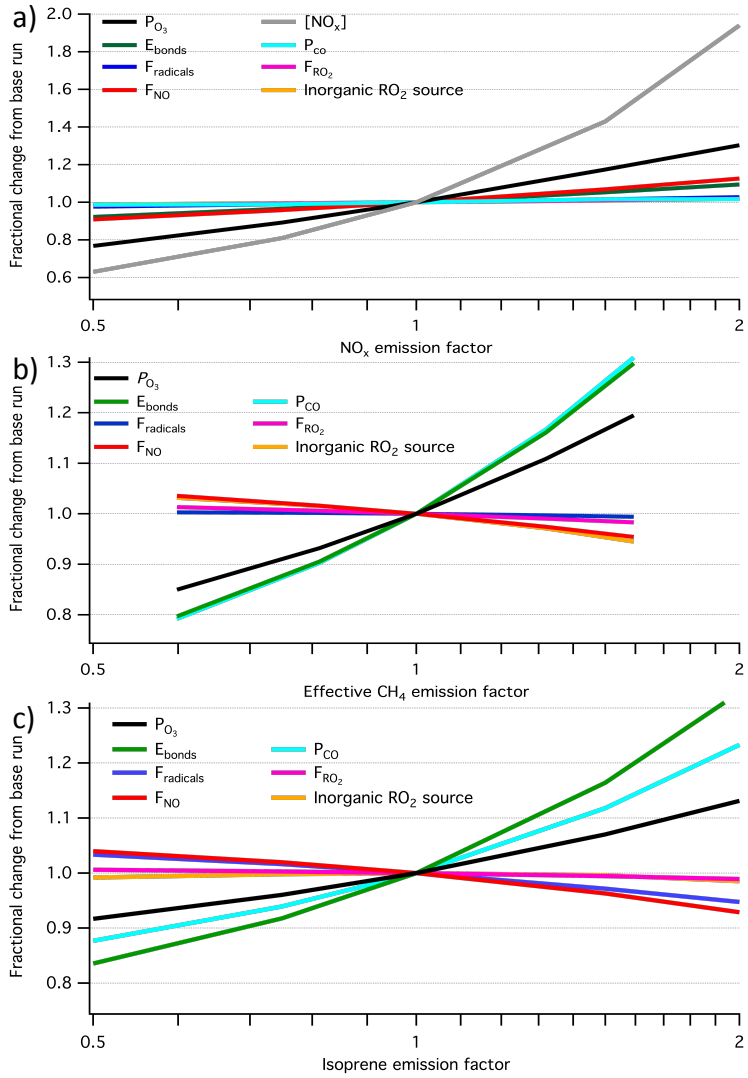

Figure 5. Fractional change in new P_sO_3 diagnostic parameters from base run against changing NO_x emission (a); effective CH_4 emission (b); and isoprene emission (c).

The response of F_{NO} to changes in NO_x emissions is also dampened relative to the change in NO_x emissions. This is due to spatial variability in F_{NO}, which is not affected uniformly by changing NO_x emissions. Figure 6 shows the probability distribution of F_{NO} values across all model grid boxes for the base simulation and the half and doubled NO_x emission simulations (black, blue and red lines respectively). For example, in a grid-box in the continental boundary layer where RO_2 reacts overwhelmingly with NO, doubling the NO_x emission may move F_{NO} from 0.90 to 0.95 but it can't double it. Similarly, in the remote boundary layer where RO_2 reacts overwhelmingly with other RO_2 doubling NO_x emissions may move F_{NO} from 0.3 to

0.4 but again it doesn't double. Thus the geographical spread of NO_x chemistry limits the change in F_{NO} caused by changing NO_x emissions. The spatial variability in the new P_sO_3 diagnostic parameters shows that this approach has significant potential in the analysis of regional O_3 budgets as well as global.

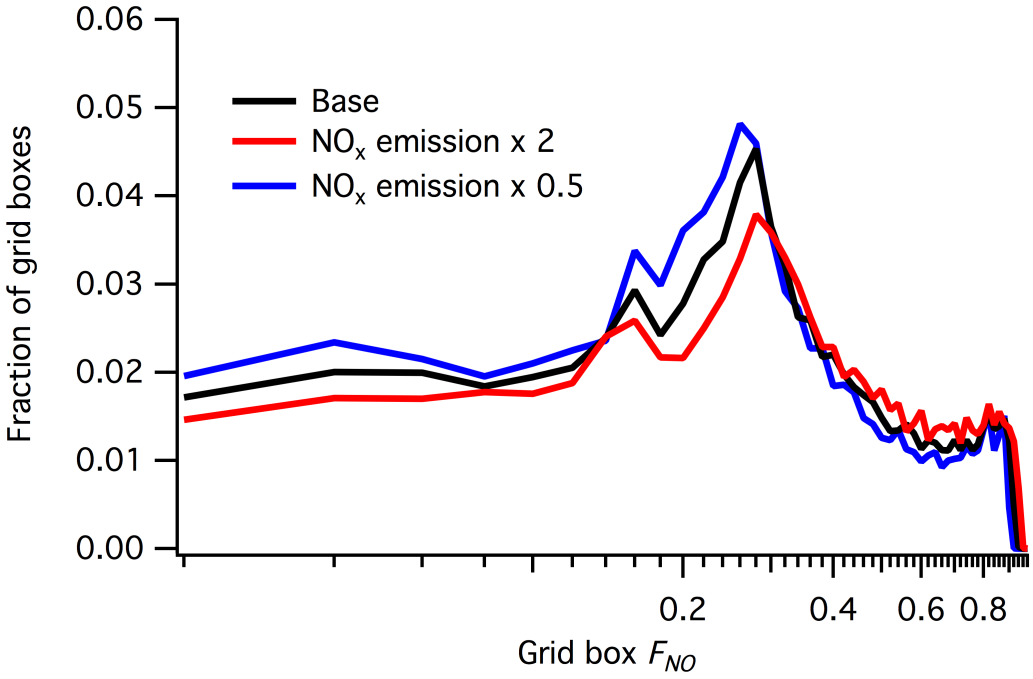

Figure 6. Effect of NO_x emission on distribution of F_{NO} values (log scale). F_{NO} values for each model grid box in the base and NO_x emission x 0.5 and x 2 simulations, split into 50 x 0.02 width bins.

4.1.2 Impact of changing NO_x emission on E_{bonds}

Figure 4a(ii) shows that 60% of the response in P_sO_3 to changing NO_x emission is due to factors other than F_{NO}, with 40% of the increase due to changes in the emissions (E_{bonds}: 32%) and chemical production (P_{bonds}: 8%) of oxidizable bonds. This increase in E_{bonds} is surprising given VOC emissions are unchanged in these simulations. However, increasing NO_x emissions results in an increased OH concentration in the model, which then leads to an increase in CH_4 oxidation. Methane (CH_4) concentrations are fixed in GEOS-Chem, resulting in an increase in the effective CH_4 emission as OH concentrations increase, causing an increase in the total bond emission (E_{bonds}). Figure 7 shows the response of effective CH_4 bond emission to global mean OH concentration as it changes with global mean NO_x concentration.

More CH_4 oxidation also leads to more CH_2O production and in turn more CO production (P_{CO}), accounting for a significant fraction of the increase in this term.

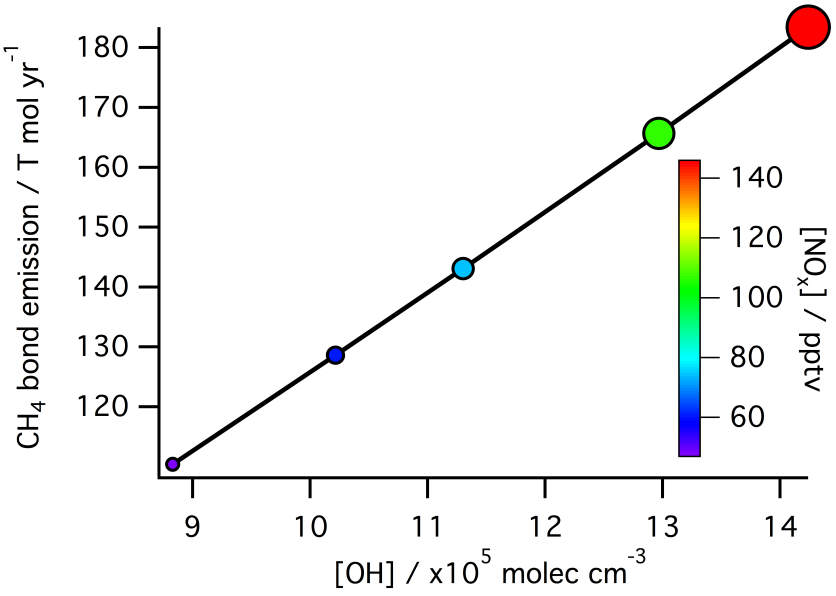

Figure 7. Effective CH_4 emissions as a function of global mean OH concentration, for simulations where NO_x emissions were changed. Marker size and colour indicate global NO_x concentration.

4.1.3 Impact of changing NO_x emission on $F_{radicals}$, F_{RO2} and *I*

The fraction of radicals produced from bond oxidation ($F_{radicals}$) and the fraction of those radicals which are RO_2 (F_{RO2}) show slight positive increase with NO_x emission, accounting for 9% and 6% of the change in P_sO_3 respectively. This reflects changes in the partitioning of the fate of the oxidisable bonds, and is largely due to the changes in OH. As OH increases with NO_x emission, the rate of chemical oxidation of bonds increases at the expense of other losses, in particular deposition. The inorganic RO_2 source term (*I*) also correlates with NO_x emission, as it is largely determined by the concentrations of OH and O_3. This change accounts for 5% of the observed change in P_sO_3.

Thus, with this new diagnostic methodology it is evident that only 40% of the model O_3 production response to changing NO_x emission is due to the direct effect of increasing NO concentration on the rate of RO_2 + NO reactions. Another 40% is due to fixing the concentration of CH_4 within the model, with the final 20% due to the increased OH concentration competing for the available oxidisable bonds and resulting in increased RO_2 production.

4.2 Changing effective CH_4 emissions

As Fig. 2 shows CH_4 to be the largest single source of oxidisable bonds, this section investigates the response of the O_3 production diagnostics to changing CH_4 emissions. Figure 4b shows the O_3 production diagnostics response to varying the CH_4 emission rate within the model. As the model uses prescribed CH_4 concentrations, these were varied by factors of between 0.5 and 2 from the base simulation and the CH_4 emission diagnosed from the loss rate of CH_4 to reaction with OH, the only CH_4 loss in the model. We describe this as the effective CH_4 emission.

As effective CH_4 emission increases, O_3 production also increases. The standard diagnostic (Fig.4b(i)) shows that this increase occurs through an increased rate of reaction of HO_2 and CH_3O_2 with NO, as would be expected as these are the RO_2 produced during CH_4 oxidation. The rate of other RO_2 + NO reactions actually decreases slightly as CH_4 emissions increase, due to lower OH concentrations and increased competition for NO from HO_2 and CH_3O_2. The new diagnostic (Fig.4b(ii)), however, shows the increase in O_3 production with increasing effective CH_4 emission is not simply a result of more HO_2 and CH_3O_2.

4.2.1 Impact of changing effective CH_4 emission on F_{NO}

The observed change in P_sO_3 is around one third smaller than would be expected from the increase in the oxidisable bond emission (E_{bonds}) and bond production (P_{bonds}) terms alone. This is due to a countering decrease in the other efficiency parameters with increasing effective CH_4 emission. Figure 5b shows the fractional change in all the efficiency parameters as a function of the changing effective CH_4 emission. The decrease in the fraction of RO_2 reacting with NO to produce NO_2 (F_{NO}) is driven by increasing O_3 concentrations, which push the NO/NO_2 ratio towards NO_2. This reduces the availability of NO to react with RO_2 thereby reducing O_3 production. This shift in the NO/NO_2 ratio also increases NO_x loss within the model with increasing CH_4 emission, as the increased CH_4 oxidation increases RO_2 concentrations resulting in larger losses of NO_2 via compounds such as peroxyacetyl nitrate (PAN) and peroxynitric acid (PNA).

4.2.2 Impact of changing effective CH_4 emission on E_{bonds}

Increasing the effective CH_4 emission results in an increase in E_{bonds}. Changing the fraction of total emitted oxidisable bonds from CH_4 does however have significant

consequences on the loss mechanisms of these bonds, which influences the other efficiency parameters. Figure 8 show the split of oxidisable bond loss mechanisms in the base simulation and those with the CH_4 concentration fields multiplied by 0.5 and 2. As the effective CH_4 emission increases the fraction of bonds lost via OH decreases, despite the actual number of oxidisable bonds lost to OH increasing. A larger fraction of bonds are therefore lost via the other mechanisms shown in Fig. 8 rather than reaction with OH. As CH_4 removal occurs predominantly in the free troposphere, increasing the effective CH_4 emission also results in a reduction in the fraction of oxidisable bonds lost via deposition. The largest fractional increase in bond loss mechanism with increasing effective CH_4 emission is for photolysis, with the increase in the "other" fraction due to increased loss of bonds to the stratosphere with increasing CH_4.

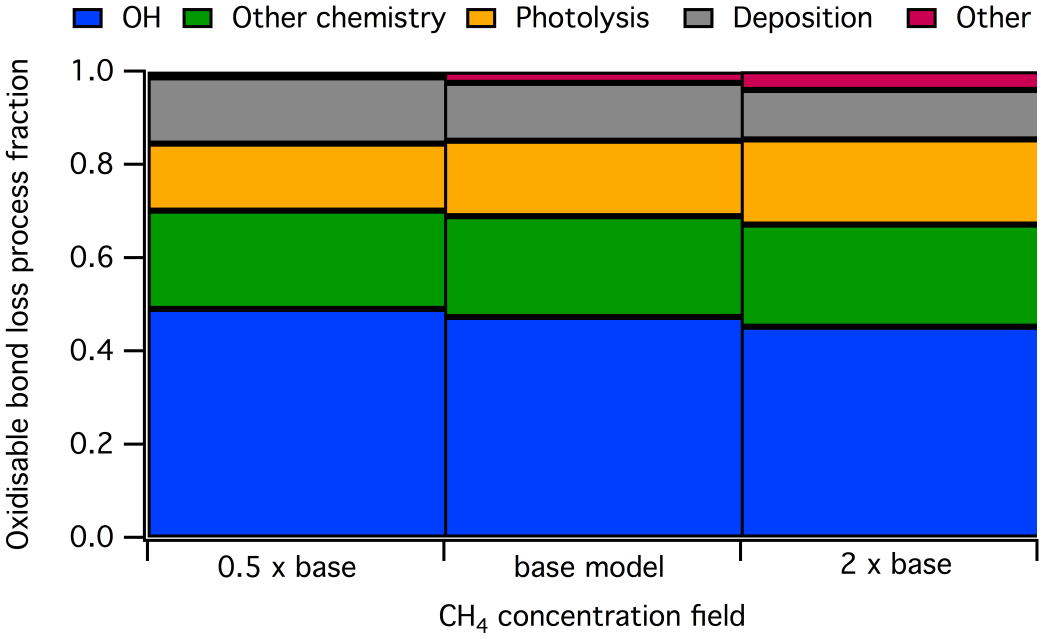

Figure 8. Oxidisable bond loss mechanism fractions under changing effective CH_4 emissions (0.5 x CH_4 concentration field, base simulation and 2 x CH_4 concentration field).

4.2.3 Impact of changing effective CH_4 emission on $F_{radicals}$, F_{RO2} and *I*

The fraction of oxidisable bonds that goes on to produce radicals ($F_{radicals}$) and the fraction of these that are RO_2 (F_{RO2}) also decrease with increasing effective CH_4 emissions. This is due to decreasing global OH concentration resulting from increased loss by reaction with CH_4 and a decreasing NO concentration. This favours bond loss

via pathways that produce less RO_2 (e.g. CH_2O photolysis). The long lifetime of CH_4 compared with the majority of other sources of oxidisable bonds, also results in a decrease in the fraction of bonds lost to deposition as total bond oxidation increases fractionally in the free troposphere where deposition is a less significant loss mechanism than in the boundary layer.

4.3 Changing isoprene emission

The species through which the oxidisable bonds are emitted has a significant impact on O_3 production, due to their subsequent removal mechanisms. For example, in a simulation where the only emission of oxidisable bonds is CO, $F_{radicals}$ is 0.5 and F_{RO2} is 1 as the only CO sink is reaction with OH to produce one HO_2 (OH + CO → HO_2 + CO_2). The CO coordinate bond, which in theory has the potential to produce 2 radicals, only produces 1 radical, which is an RO_2.

Isoprene has the most complex chemistry in the model and is the second largest source of bonds into the atmosphere after CH_4 (Fig. 3). Figure 4c shows the response of the two O_3 production diagnostics to varying the isoprene emission within the model. The standard diagnostic (Fig.4c(i)) shows that the most significant increase in PO_3 from increasing isoprene emissions is from NO + HO_2 and non-CH_3O_2 peroxy radicals, with a smaller increase from CH_3O_2. The new P_sO_3 diagnostic (Fig.4c(ii)) again provides more insight, showing significant offsetting of around a half between the terms.

4.3.1 Impact of changing isoprene emission on F_{NO}

The increased isoprene emission leads to a similar change in the magnitude of the total number of oxidisable bonds emitted (E_{bonds}) as the simulations in which effective CH_4 emission were varied. However, the countering decrease in all of the efficiency parameters is much larger for isoprene than for CH_4. Figure 5c shows the fractional change in the new P_sO_3 ozone production diagnostic parameters as a function of isoprene emissions compared to the base simulation. The change in F_{NO} is due to both a decrease in global mean NO_x concentrations with increasing isoprene and the spatial distribution of isoprene emissions. The majority of global isoprene emissions are in regions with low NO_x emissions, and thus low values of F_{NO}. Figure 9 shows a decrease in global mean NO_x, and global mean OH concentrations with increasing isoprene emissions, however, the effect is less than that seen when CH_4 is responsible

for the same increase in oxidisable bond emission. This is due in a large part to the spatial scales over which the two compounds impact.

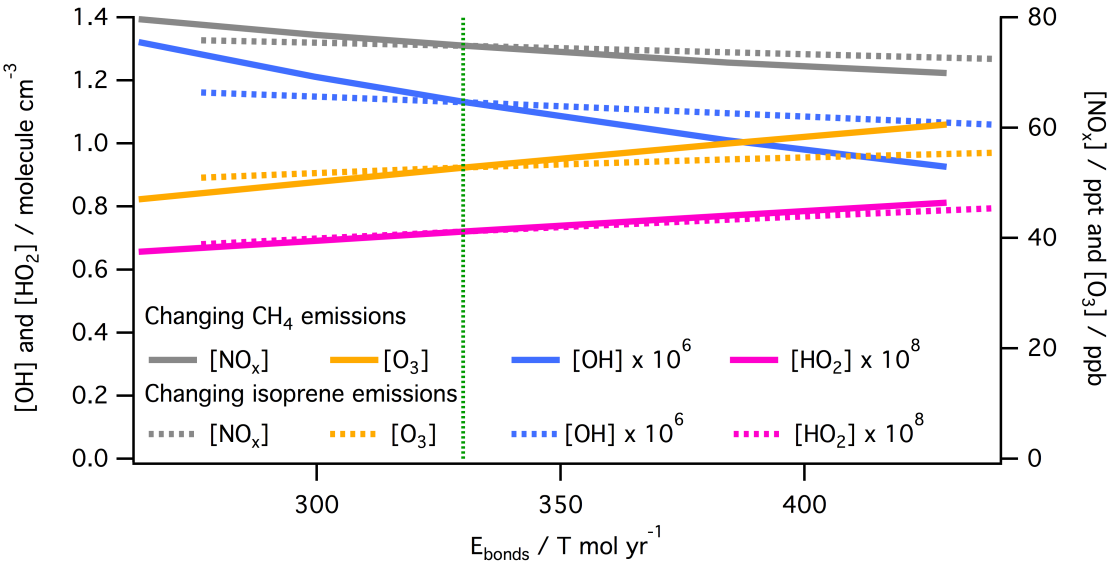

Figure 9. The effect of oxidisable bond parent species on OH, HO_2, O_3 and NO_x concentrations. Global mean [OH], [HO_2], [O_3] and [NO_x] for simulations where the effective CH_4 emission (solid lines) and isoprene emission (dashed lines) were changed, against model E_{bonds}. The dashed vertical green line indicates E_{bonds} in the base simulation (330 T mol yr^{-1}).

4.2.2 Impact of changing isoprene emission on E_{bonds}

As isoprene is the second largest source of oxidisable bonds (Fig. 3), increasing the isoprene emission results in a significant increase in E_{bonds}. Differences in both the spatial distribution of emissions and the oxidation chemistry of isoprene and CH_4, however, means that the impact of the increases in E_{bonds} on O_3 production are significantly different for the two compounds. This is predominantly because the fraction of oxidisable bonds that are physically deposited for isoprene is high compared to those emitted as CH_4. This increase is due to i) the higher solubility of isoprene oxidation products compared to those of CH_4, and ii) the higher reactivity of isoprene means its oxidation occurs in the boundary layer where both dry and wet deposition is most effective.

Figure 10 shows the fate of oxidisable bonds in the base simulation and those with the isoprene emissions multiplied by 0.5 and 2. The complex myriad of products formed during the isoprene oxidation mechanism also results in the production of many

highly oxygenated multifunctional compounds with high Henrys law solubility constants, meaning they are more readily lost to deposition.

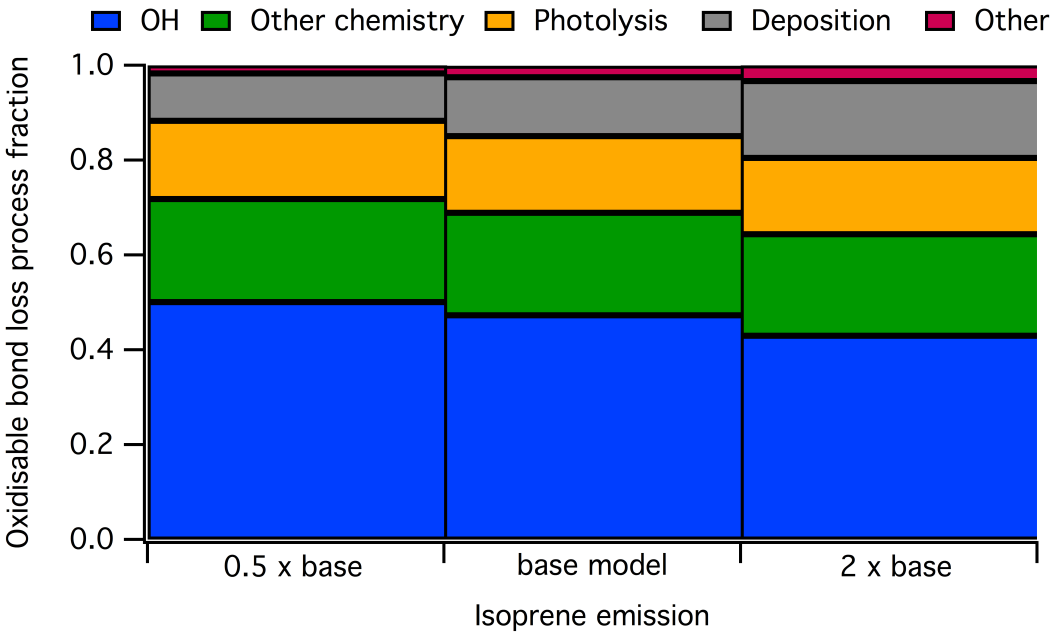

Figure 10. Oxidisable bond loss mechanism fractions under changing isoprene emissions.

Increasing the isoprene emission also has a slight offsetting impact on the effective CH_4 emission, as increased isoprene concentrations decrease OH concentrations, and thus decrease the effective CH_4 emission. A doubling in isoprene emission causes a 6% reduction in the effective emission of CH_4.

4.3.3 Impact of changing isoprene emission on $F_{radicals}$, F_{RO2} and I

As shown in Fig. 3c(ii), increasing the isoprene emission results in a reduction in all P_sO_3 efficiency parameters. The reductions in $F_{radicals}$ is due to the higher fraction of oxidisable bonds that are lost via non-radical forming pathways (e.g. deposition) for isoprene relative to the other main oxidisable bond emission sources CH_4 and CO. The slight decreases of F_{RO2} and I with increasing isoprene emission are predominantly due to changes in OH and NO_x (Fig. 9).

The complex chemistry of isoprene oxidation combined with the spatial distribution of isoprene emissions means the increase in O_3 production due to increases in isoprene emissions is roughly half what might be expected from the increase in oxidisable bond emission alone (i.e. if the increase was *via* CO instead of isoprene).

5. Conclusions

We have shown that this bond-focussed approach to O_3 production provides a significantly more detailed understanding of the processes involved. The role of modelled VOC emissions and O_3 burden has been reported previously [*Wild*, 2007; *Young et al.*, 2013]. However previous efforts extending this to a general process led approach has not been successful. This new approach provides a tool with which the processes controlling O_3 production can be investigated, and a metric by which different emissions can be compared. For example, the differing chemistry of isoprene and CH_4 shows that even though their emissions of carbon mass are comparable, the atmosphere responds in different ways, with the isoprene bonds being less effective in producing O_3 than CH_4 bonds. By quantifying multiple steps in the O_3 production process, competing changes in the system become apparent (as shown in Fig. 4b(ii) and c(ii)) and are thus testable. This enables the effect of model approximations on O_3 production to be quantified (e.g. the effect of NO_x on CH_4 emissions when using CH_4 concentration fields).

This new diagnostic also points towards the importance of observational datasets for assessing our understanding of tropospheric chemistry. Although the budget presented in Fig. 2 provides an annually integrated global estimate it points towards local comparisons that can be made to assess model fidelity. Comparisons, both their magnitude and their ratios, between observed and modelled bond concentration, bond emission and loss fluxes (e.g. OH reactivity [*Yang et al.*, 2016] or depositional fluxes

508 [*Wesely and Hicks*, 2000]), and O_3 production [*Cazorla and Brune*, 2010] would all
509 provide comparisons for outputs from the P_sO_3 diagnostic and help assess model
510 performance.

511 Future work is necessary to identify the usefulness of this approach on smaller spatial
512 and temporal scales. For regional modelling scale, the transport flux of bonds into the
513 domain would need to be considered alongside the emissions of bonds. However, this
514 might help to disentangle O_3 production due to local VOC emissions from that due to
515 VOC emissions outside of the domain. This bond focussed approach may also have
516 usefulness on shorter timescales. For example, when considering vertical fluxes in and
517 out of the boundary layer, a bond centred approach could help. What fraction of the
518 bonds emitted at the surface are exported to the free troposphere. If a measurement of
519 reactivity flux could be made this could be tested experimentally.

520 Another potentially important application is in model-model comparisons. Increases
521 in our understanding of why different models calculate different O_3 production and
522 burdens has been slow [*Stevenson et al.*, 2006; *Wu et al.*, 2007; *Young et al.*, 2013].
523 Although a complete tagging like that described here is unlikely to occur for all of the
524 models involved in the comparison, a small number of additional diagnostics is likely
525 to produce a significantly better understanding of the models. Diagnosing (1) the total
526 bond flux (direct emissions plus the flux for those species kept constant), (2) the rate
527 of production of RO_2 and (3) the rate of production of O_3, could help differentiate why
528 certain models produce more or less O_3 than others. The ratios between these fluxes
529 would help identify what aspect of the emissions of chemistry differs between the
530 models.

References

Atkins, P. W., and J. De Paula (2014), *Atkins' Physical chemistry*, 10th ed., Oxford University Press.

Cazorla, M., and W. H. Brune (2010), Measurement of ozone production sensor, *Atmos. Meas. Tech.*, *3*(3), 545–555, doi:10.5194/amt-3-545-2010.

Crutzen, P. J. (1971), Ozone production rates in an oxygen-hydrogen-nitrogen oxide atmosphere, *J. Geophys. Res.*, *76*(30), 7311–7327, doi:10.1029/JC076i030p07311.

Kroll, J. H. et al. (2011), Carbon oxidation state as a metric for describing the chemistry of atmospheric organic aerosol., *Nat. Chem.*, *3*(2), 133–139, doi:10.1038/nchem.948.

Larson, R. A., and K. A. Marley (1999), Singlet oxygen in the environment, *Environ. Photochem.*, *2*, 123–136.

Levy, H. (1973), Photochemistry of minor constituents in the troposphere, *Planet. Space Sci.*, *21*(4), 575–591, doi:10.1016/0032-0633(73)90071-8.

Mao, J., F. Paulot, D. J. Jacob, R. C. Cohen, J. D. Crounse, P. O. Wennberg, C. A. Keller, R. C. Hudman, M. P. Barkley, and L. W. Horowitz (2013), Ozone and organic nitrates over the eastern United States: Sensitivity to isoprene chemistry, *J. Geophys. Res. Atmos.*, *118*(19), 1–13, doi:10.1002/jgrd.50817.

Nguyen, M. T., R. Sumathi, D. Sengupta, and J. Peeters (1998), Theoretical analysis of reactions related to the HNO2 energy surface: OH + NO and H + NO2, *Chem. Phys.*, *230*(1), 1–11, doi:10.1016/S0301-0104(97)00383-2.

Stevenson, D. S. et al. (2006), Multimodel ensemble simulations of present-day and near-future tropospheric ozone, *J. Geophys. Res. Atmos.*, *111*(8), doi:10.1029/2005JD006338.

Wesely, M. L., and B. B. Hicks (2000), A review of the current status of knowledge on dry deposition, , *34*.

Wild, O. (2007), Modelling the global tropospheric ozone budget: exploring the variability in current models, *Atmos. Chem. Phys.*, *7*, 2643–2660, doi:10.5194/acpd-7-1995-2007.

561 Wu, S., L. J. Mickley, D. J. Jacob, J. A. Logan, R. M. Yantosca, and D. Rind (2007),
562 Why are there large differences between models in global budgets of
563 tropospheric ozone?, *J. Geophys. Res. Atmos.*, *112*(5), 1–18,
564 doi:10.1029/2006JD007801.

565 Yang, Y., M. Shao, X. Wang, A. C. Nölscher, S. Kessel, A. Guenther, and J. Williams
566 (2016), Towards a quantitative understanding of total OH reactivity: A review,
567 *Atmos. Environ.*, *134*(2), doi:10.1016/j.atmosenv.2016.03.010.

568 Young, P. J. et al. (2013), Pre-industrial to end 21st century projections of
569 tropospheric ozone from the Atmospheric Chemistry and Climate Model
570 Biogeosciences Intercomparison Project (ACCMIP), *Atmos. Chem. Phys.*,
571 *13*(10), 5277–5298, doi:10.5194/acp-13-5277-2013.

572

573 **Author contributions**

574 All work presented here was conceived by P.M.E. and M.J.E. The implementation,
575 model simulations and analysis were carried out by P.M.E., and the manuscript was
576 written by P.M.E. with substantial input from M.J.E..

577 **Additional information**

578 The authors declare no competing financial interests.

579 **Acknowledgements**

580 P.M.E. was supported by NERC Grant NE/K004603/1. This work was also supported
581 by the NERC funded BACCHUS project (NE/L01291X/1). GEOS-Chem
582 (www.geos-chem.org) is a community effort and we wish to thank all involved in the
583 development of the model.